Measurement of Bending Stresses in Shells of Arbitrary Shape Using the Reflection Moiré Method

by C. A. Sciammarella, B. Trentadue and F. M. Sciammarella

ABSTRACT—The basic equation for fringe formation in the case of reflection moiré applied to surfaces of arbitrary curvatures is derived. A practical point-by-point solution for the application of this method is introduced, and the corresponding simplified equations are given. The technique is applied to an industrial problem, the stress analysis of a shell-shaped door.

KEY WORDS—Reflection moiré, stress analysis, shells

Nomenclature

P_o = projected point of the grating
P = point of the initial shell surface where the beam coming from P_o is reflected
Q = point of the deformed shell surface where the beam coming from P_o is reflected
R = point of the image plane corresponding to point P_o before deformation
P' = point of intersection of plane π with the normal from point P
Q' = point of intersection of plane π with the normal from point Q
T = point of the image plane corresponding to P_o after deformation
$\mathbf{r_P}$ = position vector of point P
$\mathbf{r_Q}$ = position vector of point Q
$\mathbf{r_R}$ = position vector of point R
$\mathbf{r_T}$ = position vector of point T
$\mathbf{r_{PR}}$ = unit vector that defines the line PR
$\mathbf{r_{PP'}}$ = unit vector that defines the line PP'
$\mathbf{r_{QQ'}}$ = unit vector that defines the line QQ'
$\mathbf{r_{QT}}$ = unit vector that defines the line QT
$\mathbf{I_0}$ = unit vector that defines the direction of illumination
$\mathbf{n_P}$ = normal to the initial surface at point P
$\mathbf{n_Q}$ = normal to the deformed surface at point Q

A method for obtaining the partial slopes of flexed surfaces was introduced by Ligtenberg.[1] This method was extensively used at the Netherlands Organization of Applied Scientific Research for the study of complex plate systems. Reider and Ritter[2] proposed a modification of this method. Both methods use a grating that is focused on the image plane of a camera via a reflecting model surface. Pedretti[3] proposed an alternative technique in which a grating is projected on an image plane via reflection on a model. A number of optical setups to obtain partial slopes using reflecting surfaces were proposed by Theocaris.[4] More recently, Sciammarella and Combel[5] showed that all of the techniques described above are forms of shearing interferometry. Theocaris[6] and Osgerby[7] proposed extensions of the moiré reflecting technique to cylindrical shells. Kamaritova[8] analyzed the application of reflection moiré to shells. A very general discussion of the application of reflection moiré to shells was offered by Gambarova *et al.*,[9] who proposed a method based on iteration to obtain local rotations from moiré patterns resulting from the reflections of gratings of shell surfaces. Numerical examples were presented only for simple shapes as cylinders and spheres. Ritter and Schulte[10] derived equations for fringe patterns corresponding to shells of arbitrary shape. No actual applications were provided.

In this paper, a point-by-point reflection moiré technique is proposed and applied to the study of a reflecting shell.

Derivation of the Fundamental Relationships

The general equations for the formation of fringes after the reflection of a grating on a convex surface of arbitrary shape are derived from geometrical optics. These general equations will be simplified for the particular method of observation proposed in this paper. The extension to concave surfaces is immediate and requires only the use of the corresponding imaging optics.

Figure 1 shows the schematic representation of the optical system. A cross grating is illuminated by monochromatic collimated light. The image of the grating is received on a plane π after reflection on an arbitrary convex surface $S_o(x, y, z)$. To simplify expressions, the plane xy, the plane of the grating and the image plane are chosen to be parallel to each other. The surface is loaded and after deformation becomes the surface $S_d(x, y, z)$. A point P_o of the grating is imaged on the point R after reflection at the point P. After deformation, P_o is imaged onto point T via reflection on point Q of S_d. The following nomenclature is introduced. $\mathbf{I_0}$ is the unit vector defining the incident illumination beam, $\mathbf{n_P}$ is the vector normal to the surface S_o at P, $\mathbf{n_Q}$ is the vector normal to S_d at Q, $\mathbf{r_{PR}}$ is the reflected beam at P, $\mathbf{r_{QT}}$ is the reflected beam at Q and $\mathbf{r_{PP'}}$ is the perpendicular from point P to the plane π. From the law of reflection, one can conclude that

C. A. Sciammarella (SEM Member) is a Professor, Illinois Institute of Technology, Chicago, IL 60616. B. Trentadue is an Assistant Professor, Politecnico di Bari, 70126 Bari, Italy. F. M. Sciammarella (SEM Member) is a Research Associate, Illinois Institute of Technology, Chicago, IL 60616.

Original manuscript submitted: February 11, 1999.
Final manuscript received: April 25, 2000.

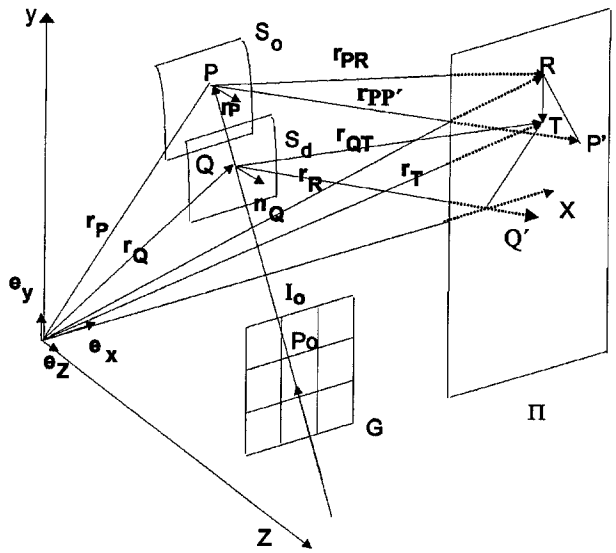

Fig. 1—Coordinate system for the analysis of the image formation in reflection moiré

$\mathbf{I_o}$, $\mathbf{n_P}$ and $\mathbf{r_{PR}}$ are in the same plane, as well as $\mathbf{I_o}$, $\mathbf{n_Q}$ and $\mathbf{r_{QT}}$. In addition, because of the laws of reflection, the angles $\mathbf{I_o} \overset{<}{\mathbf{n}}_P = \mathbf{n_P} \overset{<}{\mathbf{r}}_{PR}$, $\mathbf{I_o} \overset{<}{\mathbf{n}}_Q = \mathbf{n_Q} \overset{<}{\mathbf{r}}_{QT}$. The illumination vector is defined by

$$\mathbf{I_o} = \cos\theta_1 \mathbf{e_x} + \cos\theta_2 \mathbf{e_y} + \cos\theta_3 \mathbf{e_z}, \tag{1}$$

where $\cos\theta_i$, $i = 1, 2, 3, \ldots$, are the direction cosines of the illumination vector. The unit reflection vector $\mathbf{r_{PR}}$ can be obtained by adding the vectors $\mathbf{I_o}$ and $\lambda_P \mathbf{n_P}$:

$$\mathbf{r_{PR}} = \mathbf{I_o} + \lambda_P \mathbf{n_P}, \tag{2}$$

where λ_P is a multiplier that can be computed from Fig. 2 by applying the cosine law,

$$|\mathbf{r_{PR}}|^2 = \lambda_P^2 |\mathbf{n_P}|^2 - 2\lambda_P(\mathbf{n_P} \cdot \mathbf{I_o}) + |\mathbf{I_o}|^2, \tag{3}$$

where $\cdot$ indicates the scalar product of the two vectors and $|\ |$ indicates the magnitude of the vector. From (3) and recalling that $\mathbf{I_o}$ and $\mathbf{r_{PR}}$ are unit vectors,

$$\lambda_P = \frac{2(\mathbf{n_P} \cdot \mathbf{I_o})}{|\mathbf{n_P}|^2}. \tag{4}$$

The normal $\mathbf{n_P}$ is given by

$$\mathbf{n_P} = \mathbf{grad}\ \mathbf{S_o}(x, y, z). \tag{5}$$

Then, considering (4),

$$\lambda_P = \frac{2\mathbf{grad}\ \mathbf{S_o} \cdot \mathbf{I_o}}{|\mathbf{grad}\ \mathbf{S_o}|^2}. \tag{6}$$

The vector position of R is given by

$$\mathbf{r_R} = \mathbf{r_P} + d_{PR}\mathbf{r_{PR}}, \tag{7}$$

where d_{PR} is the distance between the points P and R. The distance d_{PR} can be computed in the following way. The triangle $PP'R$ is a right triangle, therefore,

$$d_{PR} = \frac{d_P}{\mathbf{r_{PR}} \cdot \mathbf{r_{PP'}}}, \tag{8}$$

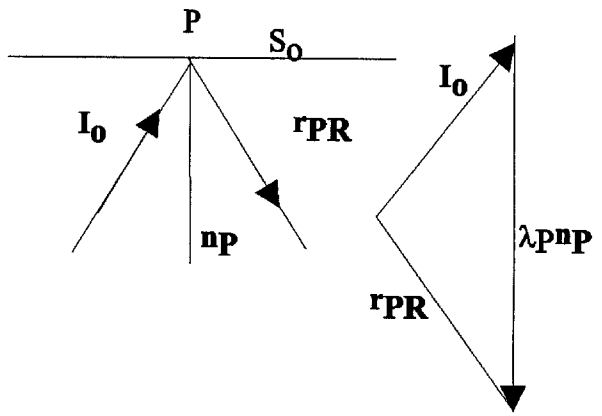

Fig. 2—Determination of λ_P

where d_P is the distance PP'. Defining D_P by the following equation,

$$\mathbf{r_{PR}} \cdot \mathbf{r_{PP'}} = D_P, \tag{9}$$

eq (7) can be written as

$$\mathbf{r_R} = \mathbf{r_P} + \frac{d_P}{D_P}\left[\mathbf{I_o} + \lambda_P\ \mathbf{grad}\ \mathbf{S_o}\right]. \tag{10}$$

Quantities similar to those defined for point P can be defined for point Q:

$$\mathbf{r_{QT}} = \mathbf{I_o} + \lambda_Q \mathbf{n_Q} \tag{11}$$

$$\lambda_Q = \frac{2[\mathbf{grad}\ \mathbf{S_d} \cdot \mathbf{I_o}]}{|\mathbf{grad}\ \mathbf{S_d}|^2}. \tag{12}$$

D_Q is defined by the following equation:

$$D_Q = \mathbf{r_{QT}} \cdot \mathbf{r_{QQ'}}, \tag{13}$$

where $\mathbf{r_{QQ'}}$ is the vector corresponding to the perpendicular line from point Q to the plane π. The distance between point Q and the plane π is called d_Q. We can write an equation for point Q similar to (10) for point P:

$$\mathbf{r_T} = \mathbf{r_Q} + \frac{d_Q}{D_Q}\left[\mathbf{I_o} + \lambda_Q\ \mathbf{grad}\ \mathbf{S_d}\right]. \tag{14}$$

The change of the position of the image point caused by the deformation of the image is

$$\mathbf{r_T} - \mathbf{r_R} = \mathbf{r_Q} - \mathbf{r_P} + \left[\frac{d_Q}{D_Q}\lambda_Q\ \mathbf{grad}\ \mathbf{S_d} - \frac{d_P}{D_P}\lambda_P\ \mathbf{grad}\ \mathbf{S_o}\right]. \tag{15}$$

Equation (15) provides the displacement of a point of a grating projected on a plane via reflection from a surface after the deformation of the surface. This equation is referred to as a global coordinate system. The displacement is a function of the grating position, the surface position, the image plane position and the gradients of the surface before and after deformation. The displacements obtained from this equation can be introduced in the moiré equations to obtain the

expressions corresponding to the moiré fringes defining the slopes of the surface. This can be done in a limited number of simple geometries, for example, a cylindrical surface. The difficulty involved in handling eq (15) in a general case can be understood with the following argument. If the contour of the projected grating is a rectangle, the resulting image after reflection on an arbitrary shell is an irregular polygon with four curved sides.

Simplification of the General Equation

In this research, we studied the bending stresses of a glass door that had the shape of an arbitrary shallow shell. To make eq (15) manageable in the short time period given to find a solution, a local formulation was chosen.

One wants to relate the displacements defined by the vectorial eq (15) to the rotations of the local coordinate system with origin at point P, the point under observation. Assuming infinitesimal rotations, the rotation vector is defined by the following equation:

$$\varphi_P = \varphi_x \mathbf{e_x} + \varphi_y \mathbf{e_y} + \varphi_z \mathbf{e_z}. \tag{16}$$

Of the three components of the rotation vector, φ_x, φ_y are the only components that can be determined by reflection moiré. The third component can not be obtained; however, in the present study this component is not required. The theory of bending of plates and shells needs only the slopes or rotations of the local base vectors $\mathbf{e_x}, \mathbf{e_y}$. These vectors must be contained in the plane tangent to the surface at the observation point.

Figure 3 shows the schematic representation of the optical setup, whereas a schematic of the portable optical bench used is shown in Fig. 4. The origin of coordinates is at point P as seen below. The illumination beam and the reflecting beam are contained in the xz plane. The z-axis is of the direction of the normal to the surface at P. The image plane is selected normal to the z-axis. For this coordinate system,

$$\lambda_P \cong \lambda_Q = 2\cos\theta. \tag{17}$$

Furthermore,

$$D_P \cong D_Q = \cos\theta \tag{18}$$

and

$$d_P \cong d_Q = d. \tag{19}$$

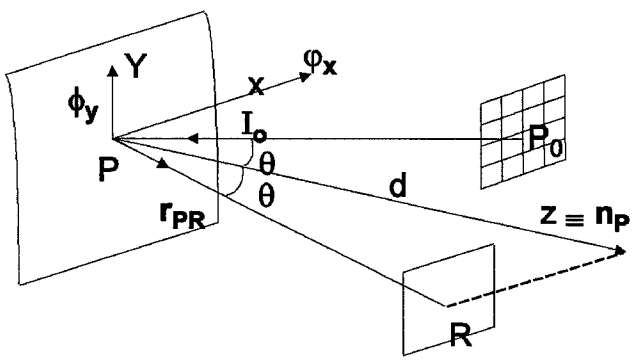

Fig. 3—Local coordinate system for the analysis of reflection moiré

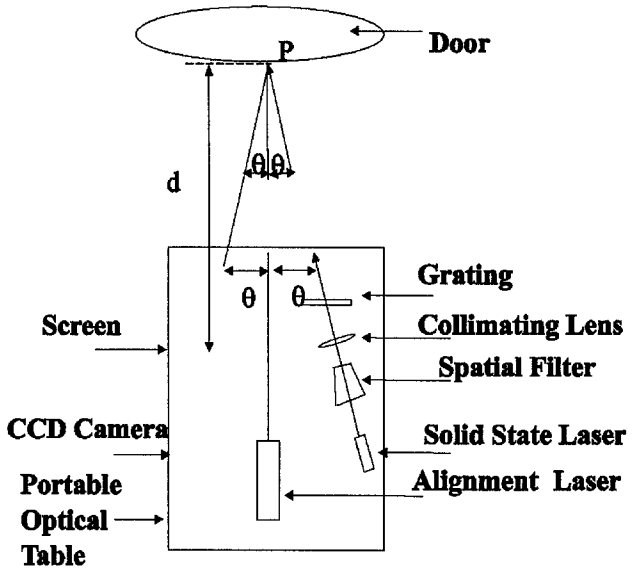

Fig. 4—Portable optical bench

Finally, (15) simplifies to

$$\mathbf{r_T} - \mathbf{r_R} = \mathbf{r_Q} - \mathbf{r_P} + 2d[\mathbf{grad\ S_d} - \mathbf{grad\ S_o}]. \tag{20}$$

To perform the local analysis, the surface near P must be described as a function of the coordinates x, y in the tangent plane. Assuming infinitesimal deformations, the deformation of the surface is given by $w(x, y)$. Consequently,

$$S_d(x, y) = S_o(x, y) + w(x, y). \tag{21}$$

According to the properties of the function gradient, (20) reduces to

$$\mathbf{r_T} - \mathbf{r_R} = \mathbf{r_Q} - \mathbf{r_P} + 2d\ \mathbf{grad\ w}(x, y), \tag{22}$$

resulting in the projection equation

$$x_T - x_R = x_Q - x_P + 2d\frac{\partial w}{\partial x} \tag{23}$$

and a similar equation for the y coordinate. From (23),

$$\frac{\partial w}{\partial x} = \frac{x_T - x_R}{2d} - \frac{x_Q - x_P}{2d}. \tag{24}$$

One can neglect the second term of (24) because it is two orders of magnitude smaller than the first. Then,

$$\frac{\partial w}{\partial x} = \frac{dx}{2d}, \tag{25}$$

where, $d_x = x_T - x_R$. Equation (25) has the classical form derived in Ref. 1. Now, using the nomenclature of the moiré method, we can express the displacement d_x:

$$d_x = \frac{\Psi_x(x, y)}{2\pi} p, \tag{26}$$

where $\Psi_x(x, y)$ is the modulation function. The modulation function represents the displacements that change the initial grating reflected on the nondeformed shell. This change is expressed as a phase angle. The quantity p is the pitch of the

grating. Finally, the change in slope of the surface is given by the following equation:

$$\frac{\partial w}{\partial x} = \frac{\Psi_x(x, y)}{2\pi} \frac{p}{2d}. \tag{27}$$

Similarly,

$$\frac{\partial w}{\partial y} = \frac{\Psi_y(x, y)}{2\pi} \frac{p}{2d}, \tag{28}$$

where $\Psi_y(x, y)$ is the modulation function corresponding to the y-direction. Equations (27) and (28) can be used by differentiating them to compute the curvatures

$$\kappa_x = \frac{\partial^2 w}{\partial x^2} \tag{29}$$

$$\kappa_y = \frac{\partial^2 w}{\partial y^2} \tag{30}$$

$$\kappa_{xy} = \frac{\partial^2 w}{\partial x \partial y}. \tag{31}$$

The curvatures can be replaced in the shell equations for bending. The membrane stresses can be obtained by printing a grating on the surface of the shell and observing the moiré fringes produced by the load.

Generalization to Coherent Optics

The above derivations are valid both for coherent and for incoherent illuminations.

An analysis similar to the one carried out in Ref. 5 can be used in this case. The final expression will be identical; however, the wave analysis introduces two important aspects of the problem.

One aspect is the fact that reflection moiré is a wave front shear interferometry method. The second aspect has to do with the self-imaging property of gratings when illuminated with coherent light. Away from the plane of the grating, the grating reproduces itself[12] at distances given by

$$z = \frac{Kp^2}{\lambda}, \tag{32}$$

where z is the distance along the normal to the grating, λ is the wavelength of the light used and $K = 1, 2, 3$. The distance between the grating that is projected and the reflecting surface must be an integer number of z computed in (32). In the following section, we apply the technique that has been presented above.

Application of the Proposed Technique to the Analysis of a Shell

The proposed technique was applied to the stress analysis of a tempered glass door. The door dimensions are shown in Fig. 5. The stresses caused by closing the door are of particular importance. These stresses were determined by applying a concentrated load on the handle that operates the door.

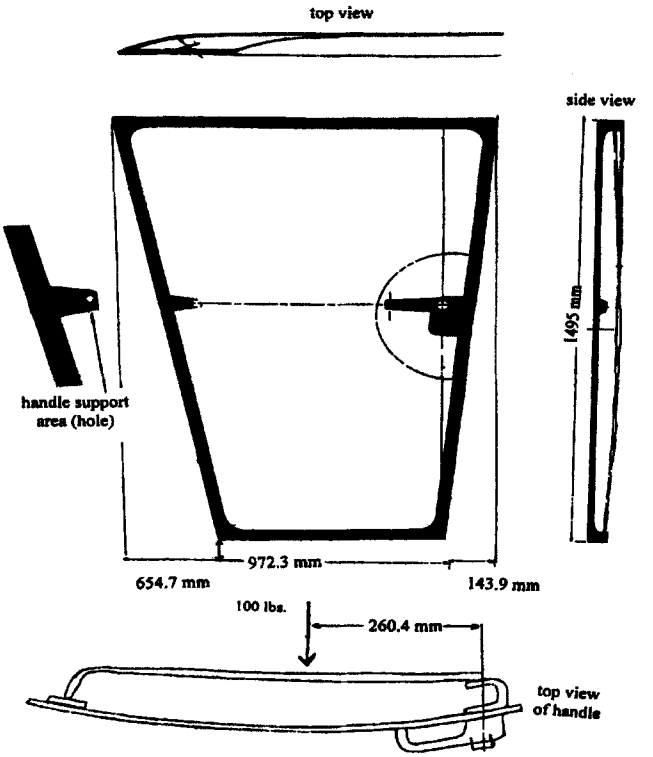

Fig. 5—Geometry of the analyzed shell

The optical measurements were carried out using a portable optical bench (see Fig. 4). The bench provides the direction of illumination and observation, schematically represented in Fig. 3. A collimated light projects a cross grating on the door surface. The reflected image is captured in a translucent screen. A CCD camera that provides the input to the signal-processing system captures the image. The alignment laser is used to set up the axis of the optical bench along the normal to the door surface. The frame supporting the door has leveling screws that can be used to give the door the required orientation at each of the measuring points. The door failure occurs in the process of closing. The process of closing the door produces two separated but related effects: (1) the glass door is forced to contact the rubber sealing of the frame, thus introducing boundary contact stresses, and (2) changes of curvature take place under the applied load. The measurements were carried out in the following conditions: door open, door closed and door closed and loaded. Because the curvatures are tensors, tensorial laws of superposition were applied to compute the final changes of curvature.

A cross grating of four lines per millimeter was used. Because the image of the grating could be observed directly, a reference grating was not used.

The measurements provide results at a given point. Actually, a small region of the shell was identified through a marking done before the measurement. Because the grating itself can be observed, the method presented in Ref. 11 was applied. The grating in the unloaded condition was recorded. The shell was loaded, and the position of the shell was modified to ensure that the normal direction of the shell with respect to the optical bench was preserved. The small changes of direction of the normal were produced by the rigid-body motion of the shell that was elastically supported at its edges on rubber gaskets. The nondeformed and deformed grating

information was processed. The fast Fourier transforms of the gratings were computed. The x-direction and y-direction information was separated by filtering in the frequency space. The wrapped phases of the grating in the x- and y-directions were computed for the loaded and unloaded conditions. The wrapped phases were subtracted, yielding the wrapped-phase differences between the loaded and unloaded conditions. The derivatives of the phase changes were computed using the method described in Ref. 13. In this case, the observation that the cross derivatives computed from the carriers in the x-direction and in the y-direction are equal indicates that the independently determined functions $\psi_x(x, y)$ and $\psi_y(x, y)$ are in good agreement within experimental error.

The stresses were computed by using the shell equations,

$$\sigma_x = \frac{Eh}{2(1-\nu^2)}\left[\frac{\partial^2 w}{\partial x^2} + \nu\frac{\partial^2 w}{\partial y^2}\right] \tag{33}$$

$$\sigma_y = \frac{Eh}{2(1-\nu^2)}\left[\frac{\partial^2 w}{\partial y^2} + \nu\frac{\partial^2 w}{\partial x^2}\right] \tag{34}$$

$$\tau_{xy} = \frac{Gh}{2}\frac{\partial^2 w}{\partial x \partial y}, \tag{35}$$

where E is Young's modulus, h is the thickness of the glass and G is the shear modulus. Figure 6 shows a view of the actual setup. The membrane stresses were not measured, since the shell was very shallow and in the regions of interest the bending stresses were much higher than the membrane stresses.

Results

Figure 5 shows the region of maximum stresses located at the handle support area. The operating handle is supported at the hole shown in Fig. 5. Figure 7 shows the shell isostatics in the region of interest. Figure 8 shows the principal stresses σ_1, and Fig. 9 provides an enlarged detail of the principal stresses σ_1 and the isostatics in the region of maximum stresses. In the above-mentioned figures, the distances are measured along the shell surface. The σ_1 stresses are bending stresses and occur on the outside face of the door. The stresses plotted in Figs. 7 through 9 correspond to the condition of door closed and loaded. The maximum stresses occur along the line of contact of the glass with the hinge of the door. Figure 10 shows the maximum stresses along the hinge area. The line designated OL (open loaded) corresponds to the total stresses resulting from closing the door with a force of 448 N (100 lbs). OU represents the stresses corresponding to the effect of conforming the glass door to the frame. Finally, UL represents the stress corresponding to the applied load and is the stress shown along the extreme left-hand line of Fig. 8.

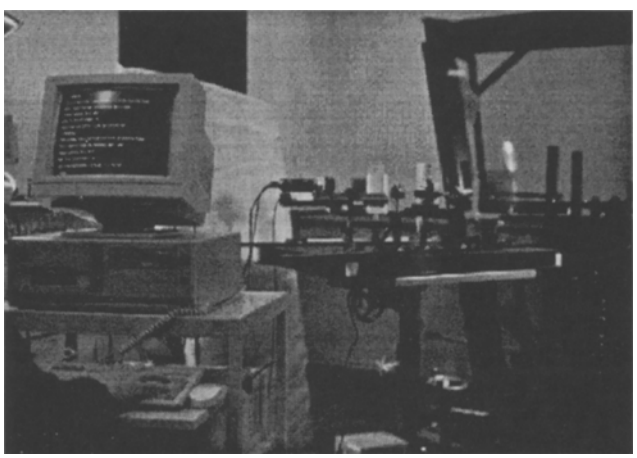

Fig. 6—View of the test setup

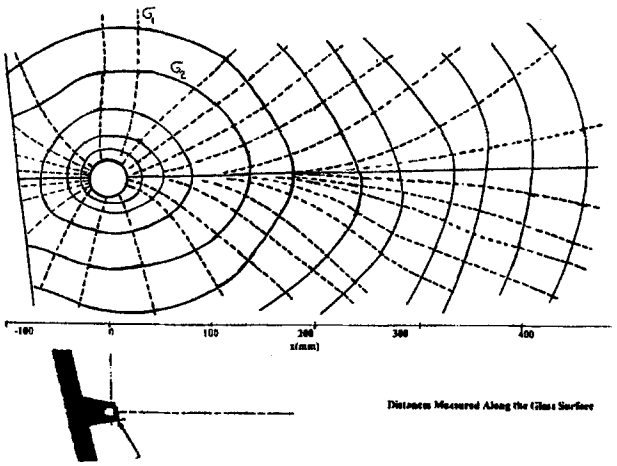

Fig. 7—Isostatics of the analyzed region

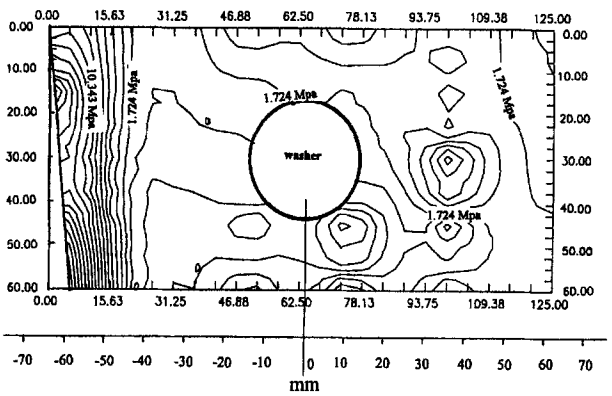

Fig. 8—Principal stresses σ_1

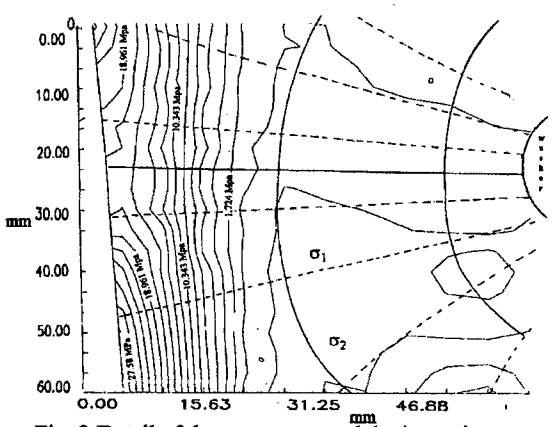

Fig. 9-Detail of the stresses σI and the isostatics

Fig. 9—Detail of the stresses σ_1 and the isostatics

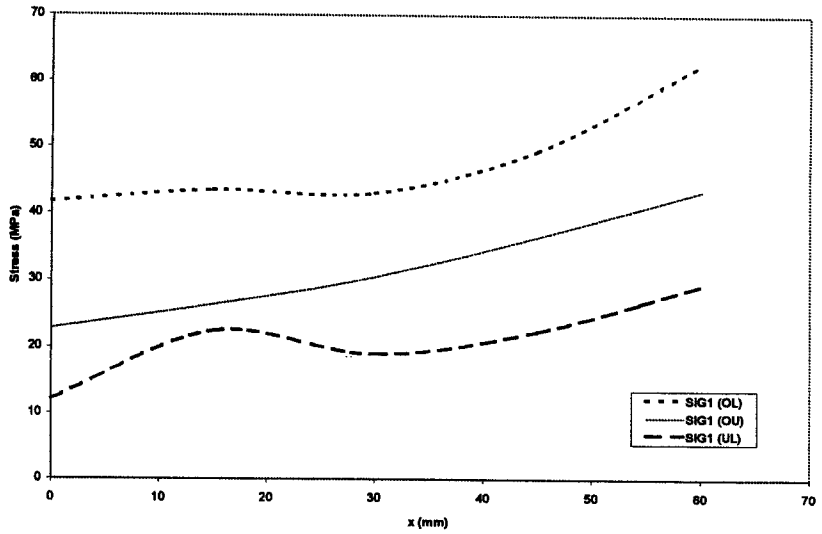

Fig. 10—Stresses σ_1 along the hinge contact area

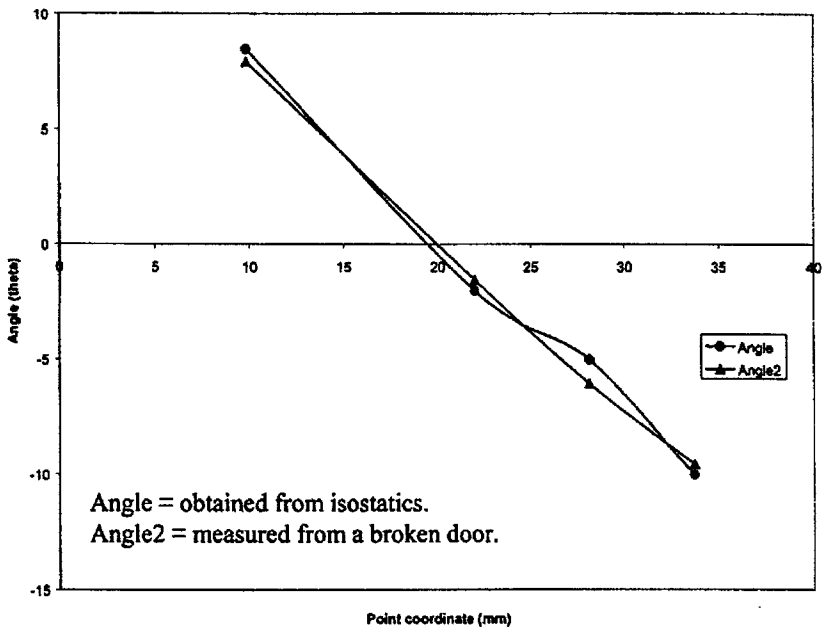

Fig. 11—Comparison between the isostatics resulting from the stress analysis and the isostatics measured in a broken door

Discussion and Conclusions

The stress analysis conducted on the door showed that the region seen at the bottom of Fig. 9 is the region of highest stress. The highest stresses occur along the line where the glass door contacts the hinge that supports the door. The residual stresses in the glass were measured photoelastically. Pieces were collected from a previously failed door and submersed in a liquid matching index for measurement. Computer-assisted photoelasticity was applied. In the region where the fracture of the door took place, the maximum residual stresses averaged 21.21 MPa (3038 psi). Adding the residual stresses to the minimum strength of the glass (41.9 MPa [6000 psi]), one obtains a modulus of rupture (63.11 MPa) that compares with the estimated maximum stress of the glass under service conditions (63.36 MPa). This result indicated that actual failure could take place in service if the appropriate adverse circumstances combine. Thus, the experimental results provided an explanation for the observed field failures.

The cracked glass remaining at the region of support of the pull bar in doors broken under service conditions has the shape of the isostatics shown around the hole in Fig. 7. This hole is where the pull bar is connected to the door. To further relate the isostatic resulting from the experimental stress analysis to the broken specimens, measurements of the direction of the cracks with respect to the normal to the edge of the door were carried out. Figure 11 shows the results.

The determination of the direction of the isostatics from the broken door requires an explanation. It is a well-known fact that brittle materials break along lines perpendicular to the minimum principal stress σ_2; this is the principal behind brittle lacquers. The above conclusion is true without residual stresses. When residual stresses are present, the mechanism of fracture is more complicated. When a crack initiates in the direction perpendicular to the maximum tensile stress, the element of volume will experience a sudden expansion because of the relaxation of the compressive residual stresses. This causes a contraction in the perpendicular direction, and a crack propagates in this direction. Cracks in the direction of the tensile isostatics, as well as cracks perpendicular to this direction, were observed in the broken door.

The preceding results indicate that the technique used in the current study provides satisfactory results, in that they are supported by observed facts. Several finite element solutions were run, and none provided good results. The difficulty in formulating an adequate finite element model lies in the elastic supporting condition at the edges of the shell and the unknown boundary conditions at the region of application of the load (the circular region shown in Fig. 9).

Acknowledgments

This research was funded by Case Corporation, whose assistance is gratefully acknowledged. The authors thank B. Singh for support and cooperation.

References

1. Ligtenberg, F.K., "The Moiré Method: A New Experimental Method for the Determination of Moments in Small Slab Models," Proceedings of the Society for Experimental Stress Analysis, **12**, *83–98 (Feb. 1954).*

2. Reider, G. and Ritter, R., "Krummungs messung an belasteten Platten nach den Ligtenbergschen Moiré Verfahren," Forschung im Ingenieurwesen, **31** *(3), 33–34 (1965).*

3. Pedretti, M., "Nouvelle Methode de Moiré Pour L'Anlyse des Plaques Flechies," Doctoral diss., Ecole Polytechnique Federale de Lausanne (1974).

4. Theocaris, P., Moiré Fringes in Strain Analysis, Pergamon Press, London, 262–278 (1969).

5. Sciammarella, C.A. and Combel, O., "Interferometric Reflection Moiré," Proceedings of the International Society for Optical Engineers: Interferometry VII, Applications, J. Pryputniewicz, G. Brown and W.P. Jupner, eds., SPIE, Bellingham, WA, 72–85 (1995).

6. Theocaris, P., Moiré Fringes in Strain Analysis, Pergamon Press, London, 1969, p:330–337.

7. Osgerby, C., "Application of the Moiré Method for Use with Cylindrical Surfaces," EXPERIMENTAL MECHANICS, **7**, *313–320 (1967).*

8. Kamaritova, M., "The Solution of Shells by the Moiré Method," Acta Technica Csav., No. 2 (1969).

9. Gambarova, P., Giovani, E., and Ronca, P., "La deformazione di modelli a doppia curvatura con il metodo del moiré per riflessione," Istituto di Scienza e Tecnica Delle Costruzioni del Politecnico di Milano Pub. No. 698 (1975).

10. Ritter, R. and Schulte, U., "Vibration Analysis by the Time Average Reflection Grating Principle," Optik, **75** *(4), 130–134 (1987).*

11. Sciammarella, C.A. and Bhat, G., "High Resolution Computer Aided Moiré," SPIE Proceedings: Part I. Moiré Techniques, Holography, Interferometry, Optical NDT and Application to Fluid Mechanics, **1554B**, *F.-P. Chiang, ed., SPIE, Bellingham, WA, 162–173 (1991).*

12. Sciammarella, C.A. and Davies, D., "Gap Effect in Moiré Fringes Observed with Coherent Monochromatic Collimated Light," EXPERIMENTAL MECHANICS, **8**, *459–466 (1968).*

13. Sciammarella, C.A. and Bhat, G., "Two Dimensional Fourier Transform Methods for Fringe Pattern Analysis," Proceedings of the Seventh International Congress on Experimental Mechanics, **12**, *Bethel, CT, 1530–1538 (1992).*